

Exploring Ink Spreading

*Patrick Emmel, Roger David Hersch
Ecole Polytechnique Fédérale de Lausanne (EPFL),
CH-1015 Lausanne, Switzerland.
Patrick.Emmel@epfl.ch, Rd.Hersch@epfl.ch*

Abstract

This study aims at exploring ink spreading, which causes significant colour deviations in ink-jet printing. We present a method for investigating this phenomenon by considering only a limited number of cases. Using a combinatorial approach based on Pólya's counting theory, we determine a small set of ink drop configurations which allows to deduce the ink spreading in all other cases. This improves the estimation of the area covered by each ink combination which is crucial in colour prediction models. Such models simplify the calibration of ink-jet printers.

Keywords: ink spreading, Pólya counting, halftones, ink-jet printing, dot gain, calibration.

Introduction

In previous publications,^{5,6} we presented a colour prediction model for halftoned samples which is based on a new mathematical formulation of the Kubelka-Munk equations. This new model requires, like Neugebauer-based methods,¹³ an estimation of the area covered by each ink density combination. This estimation needs to be computed by simulating the printing process.

In ink-jet printing, the superposition of ink drops causes a significant dot gain, i.e. a change of the covered area (see Figure 1). When ink drops are printed one over another or just partially overlap, an ink spreading process takes place. This phenomenon results from a complex physical interaction between the ink drops and the surface of the printed media. Changing the inks or the paper modifies the magnitude of the spreading and induces colour prediction errors ranging up to $\Delta E = 20$ in CIELAB.

According to observations made under the microscope, the spreading depends on the state of the surface ("wet" or "dry") and the configuration of the neighbouring impacts. In our previous study,⁶ we analysed samples made of two ink layers, and deduced a set of empirical rules describing the enlargement of the impact of an ink drop. For each ink-paper combination twelve enlargement coefficients were estimated by observing samples under the microscope. This approach lead to accurate colour predictions but it had two major drawbacks: firstly, the simulated dot shapes are not realistic; secondly, the number of different configurations and the number of enlargement coefficients increases dramatically with the number of ink layers.

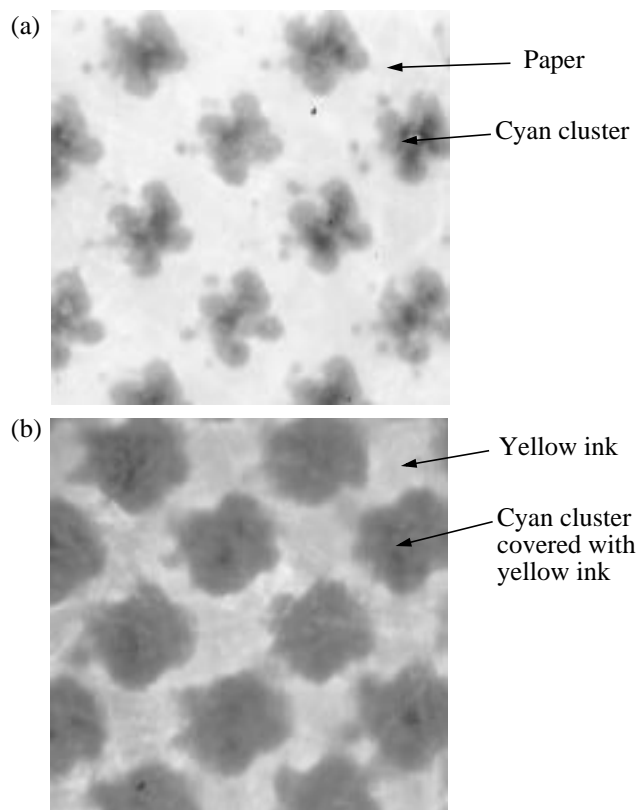


Figure 1. Microscopic views of a halftoned cyan sample (a) and of a green halftoned sample (b). The green sample (b) is made of the same cyan layer as (a) and covered with a uniform yellow layer. Note the enlargement of the cyan clusters in (b).

Therefore, a new investigation method is proposed. It is based on an impact model whose shape changes as a function of the configuration of the neighbouring impacts and of the state of the surface. Since the number of configurations is high, Pólya's counting theory is used to find a reduced set of cases whose analysis allows to deduce the spreading in all other configurations. By building samples with this reduced set, standard measuring instruments can be used to estimate the ink spreading. This information will be used by our colour prediction model in order to compute accurately the spectra of printed samples.

* Proceedings of the 8th IS&T/SID Color Imaging Conference: Color Science and Engineering, November 7-10, 2000, Scottsdale, Arizona, USA, pp. 335-341.

The impact model

In our colour prediction software,⁶ high resolution grids model the printed surface. One grid is used for each ink. The value of a grid point corresponds to the local amount of a given dye (see Figure 2). The density profile of an isolated ink impact was measured under a microscope and approximated by a parabolic function.³ The resulting ink impact model (see Figure 2) is used as a stamp. Wherever an ink drop hits the surface of the printed media, the impact model is stamped at the same location on the high resolution grid. Stamp overlapping is additive.

In a colour print using n inks, the ink combination covering a surface element at position (x, y) is given by the set of n values of the grid points (x, y) in the n superposed high resolution grids. The area covered by a given combination of n inks is estimated by counting the number of surface elements having the same set of n values.

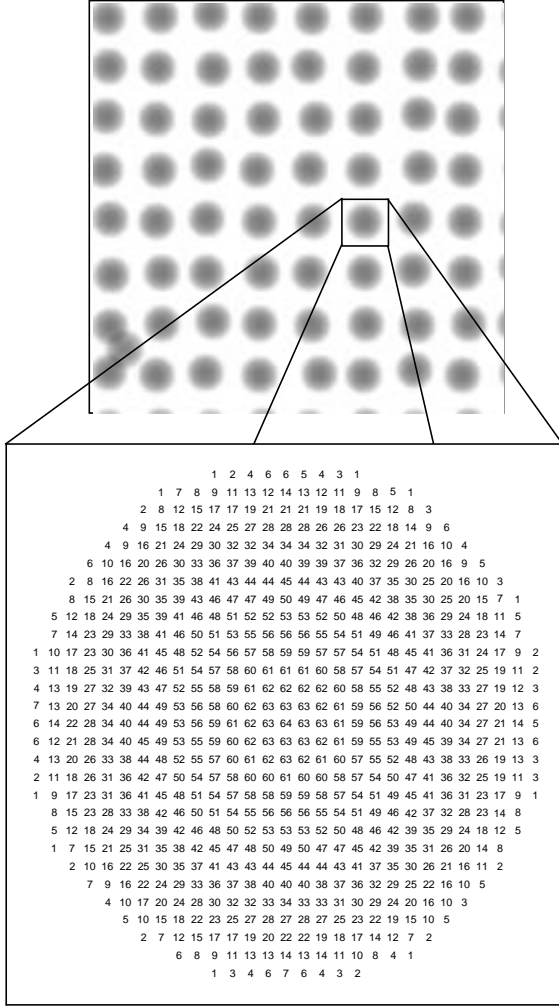


Figure 2. High resolution grid modelling the printed surface. The value of a grid point corresponds to the local amount of dye. The density profile of an isolated ink impact is parabolic.

So far, the impact model has a circular or an elliptic shape. Let us extend this model by using more sophisticated shapes. This allows to model the ink spreading phenomenon by modifying the shape of an impact according to the configuration of its neighbouring ink drop impacts and the state of the surface.

Most ink-jet printers use a hexagonal grid when printing in colour. Hence, each impact has six neighbours. Therefore, the circumference of an impact is parametrised by six vectors having a common origin at the impact centre. Each vector is oriented to the direction of the midpoint between two neighbouring impacts (see Figure 3). Let us denote r_i ($1 \leq i \leq 6$) the length of the vector which is oriented in the direction given by the angle $\theta_i = \pi/6 + (i-1) \cdot \pi/3$. The shape of the impact is approximated by a parametric curve which joins the vertices defined by the six vectors.

Let us denote $\rho = r(\theta)$ the equation in polar coordinates of this parametric curve. Since we assume that a neighbour influences only locally the shape of the impact, the parametric curve depends only on r_i and r_{i+1} when $\theta_i \leq \theta \leq \theta_{i+1}$. In order to get realistic impact shapes, we interpolate the values of the radius ρ between r_i and r_{i+1} by using a polynomial of degree three:

$$\rho = r(\theta) = 2(r_i - r_{i+1})t^3 - 3(r_i - r_{i+1})t^2 + r_i \quad (1)$$

where $t = \frac{3}{\pi} \left(\theta - \frac{\pi}{6} \right) - i$ and $\frac{\pi}{6} + (i-1) \cdot \frac{\pi}{3} \leq \theta \leq \frac{\pi}{6} + i \cdot \frac{\pi}{3}$.

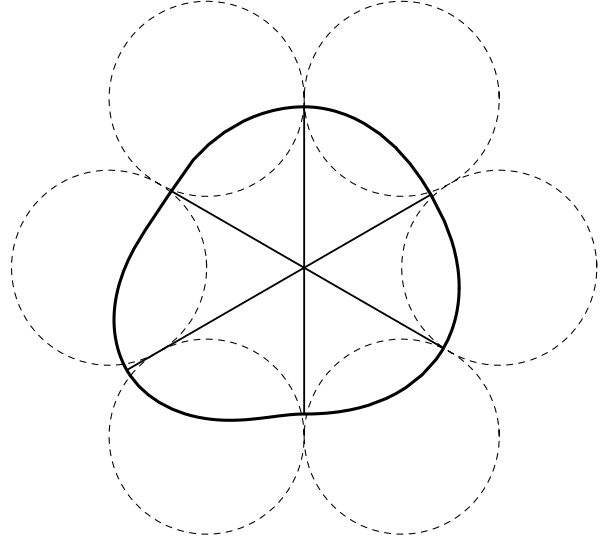


Figure 3. Six vectors define the circumference of the impact. The dashed circles indicate the locations of neighbouring impacts.

We assume that the density D at the location defined by the polar coordinates (ρ, θ) ($0 \leq \rho \leq r(\theta)$) is given by:

$$D(\rho, \theta) = D_M \cdot \left[1 - \left(\frac{\rho}{r(\theta)} \right)^2 \right] \quad (2)$$

where D_M is the density at the centre of the impact. Note that a circular impact ($r(\theta)$ constant) has a parabolic density profile as observed in our previous study.³

The amount of dye remains constant during the spreading process, only the spatial distribution is changed. Therefore, the maximal density D_M at the centre of the impact must decrease when the impact is enlarged. By integrating relation (2) over the area occupied by the impact, we get the total amount of dye within the impact (see Appendix). Since this amount must remain constant, we get the following relation for D_M :

$$D_M = D_0 \cdot \left(\frac{6r_0^2}{\sum_{i=1}^6 \left[r_i r_{i+1} + \frac{13}{140} \cdot (r_i - r_{i+1})^2 \right]} \right) \quad (3)$$

where r_0 and D_0 are respectively the radius and the maximal density at the centre of an isolated circular impact which did not spread.

This new impact model allows to simulate the spreading by changing the six r_i coefficients according to the configuration of the neighbours and the state of the surface.

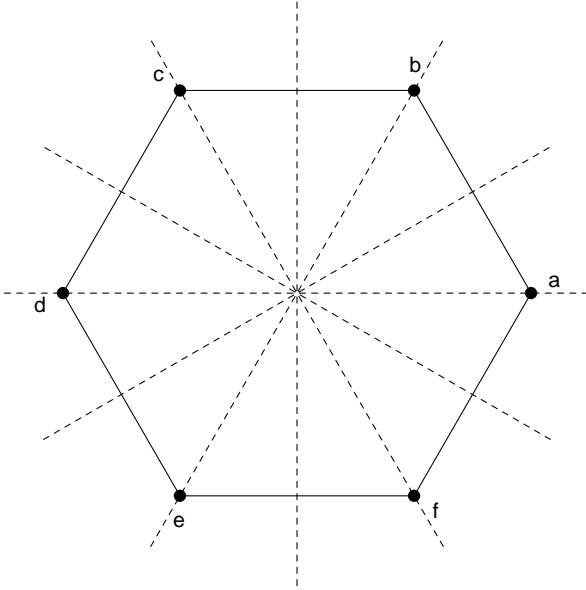


Figure 4. There are six rotations and six reflections which bring a regular hexagon onto itself.

Pólya counting

As we pointed out in the previous section, most ink-jet printers use a hexagonal grid when printing in colour. So each impact has six neighbours whose centres are the corners of a regular hexagon. In a three-ink colour print, each pixel of the printed surface is in one of the following four states: no ink,

covered with one ink drop, covered with two ink drops or covered with three ink drops. Since an impact has six neighbours, there are $4^6 = 4096$ possible neighbour configurations. On the considered centre point, a new ink drop is printed on a surface which is in one of the following three states: dry (no ink), covered with one ink drop or covered with two ink drops. Therefore, there are $3 \times 4^6 = 12288$ configurations to consider.

Among these 12288 configurations, many are equivalent by reflection or by rotation. Note that there are twelve symmetries which bring a regular hexagon onto itself: six rotations and six reflections (see Figure 4). By considering only non-equivalent configurations, the number of cases to analyse can be reduced.

At the beginning of the century, the mathematician George Pólya developed a theory for this kind of counting problem.¹¹ Later, his work was translated into English¹² and became known in the mathematical literature as ‘‘Pólya’s counting theory.’’ In the forthcoming discussion, we present only how to apply this theory to our problem. Good presentations of Pólya’s counting theory can be found in textbooks.¹

Table 1: Cycle factorisations and monomials of the group D_6 acting on the corners of the hexagon

Symmetry	Cycle factorization	Monomial
ρ_6^0	[a], [b], [c], [d], [e], [f]	z_1^6
ρ_6^1	[a,b,c,d,e,f]	z_6
ρ_6^2	[a,c,e], [b,d,f]	z_3^2
ρ_6^3	[a,d], [b,e], [c,f]	z_2^3
ρ_6^4	[a,e,c], [b,f,d]	z_3^2
ρ_6^5	[a,f,e,d,c,b]	z_6
τ_{ad}	[a], [d], [b,f], [c,e]	$z_1^2 z_2^2$
τ_{be}	[b], [e], [a,c], [d,f]	$z_1^2 z_2^2$
τ_{cf}	[c], [f], [a,e], [b,d]	$z_1^2 z_2^2$
τ_{ab}	[a,b], [c,f], [d,e]	z_2^3
τ_{bc}	[b,c], [a,d], [e,f]	z_2^3
τ_{cd}	[c,d], [a,f], [b,e]	z_2^3

As mentioned above, there are twelve geometric motions, six rotations and six reflections, which act as permutations of the corners of the regular hexagon. Let us denote ρ_6^0 , ρ_6^1 , ρ_6^2 , ρ_6^3 , ρ_6^4 and ρ_6^5 the rotations by an angle of $\theta = 0$, $\theta = \pi/3$, $\theta = 2\pi/3$, $\theta = \pi$, $\theta = 4\pi/3$ and $\theta = 5\pi/3$ respectively. Furthermore, we denote τ_{ad} , τ_{be} , τ_{cf} the reflections whose axes are the lines (ad) , (be) , (cf) respectively, and τ_{ab} , τ_{bc} , τ_{cd} the reflections whose axes are the mediators of the segments $[ab]$, $[bc]$, $[cd]$ respectively. This set of twelve symmetries with the composition operation has a

group structure:⁹ the unit element is ρ_6^0 , each symmetry has an inverse, and the composition of two symmetries is still a symmetry. Let us denote this group D_6 . The group is acting on the set of corners of the hexagon.

By applying the same operation, one of the symmetries listed in Table 1, iteratively to the hexagon, the corners follow cyclic trajectories. After a finite number of iterations, each corner gets back to the starting point. For instance, by applying iteratively the rotation ρ_6^2 to the corner (a) of Figure 4, we get the cycle $[a, c, e]$: a is first moved to c, then to e, and finally comes back to a. Note that for a given symmetry, an individual corner belongs only to one cycle. A classical result from group theory shows that each element of D_6 acting on the set of corners of the hexagon can be factorized into disjoint cycles.¹⁰ The factorisations of the elements of D_6 are listed in the second column of Table 1. The reflection τ_{cf} , for instance, is factorized into two cycles of one corner ($[c]$ and $[f]$) and two cycles of two corners ($[a, e]$ and $[b, d]$).

Let the variable z_i correspond to a cycle having i corners. To each symmetry we associate a monomial which is the product of the (z_i) 's according to the cycle factorization, as shown in the third column of Table 1. The reflection τ_{cf} is associated with $z_1 \cdot z_1 \cdot z_2 \cdot z_2 = z_1^2 z_2^2$.

The sum of the monomials divided by the number of the symmetries of the group D_6 is called the cycle index:

$$P(z_1, z_2, z_3, z_6) = \frac{1}{12} \cdot (z_1^6 + 2z_6 + 2z_3^2 + 4z_2^3 + 3z_1^2 z_2^2) \quad (4)$$

Let us denote k be the number of states in which a corner can be. According to Pólya's theory,² the number of non-equivalent hexagons is:

$$P(k, k, k, k) = \frac{1}{12} \cdot (k^6 + 2k + 2k^2 + 4k^3 + 3k^4) \quad (5)$$

Therefore, the number of non-equivalent configurations of six neighbouring ink drop impacts being in one of k states is given by $P(k, k, k, k)$. Furthermore, a new drop is printed on a surface which is in one of $(k - 1)$ states. So finally, the total number of non-equivalent configurations is:

$$N = (k - 1) \cdot P(k, k, k, k) \quad (6)$$

In colour prints using three inks, we have $k = 4$ states (no ink, one ink drop, two ink drops, three ink drops). Hence the number of non-equivalent configurations is $N = 1290$. In four-ink-printing ($k = 5$), N rises to 6020. Note that for two inks $k = 3$ and N drops to 184.

Other geometric shapes, as for instance non-regular hexagons, are mapped onto themselves by other groups of symmetries. But the same procedure can be applied to find the number of non-equivalent configurations.

Remember that Pólya's counting requires three steps: first, defining the group of symmetries acting on the set of corners, second, factorizing each permutation into cycles, and third, calculating the cycle index polynomial.

A simplified model of ink spreading

The spreading process is a complex interaction between the inks and the printed surface. It is strongly related to physical properties like wettability and solvent absorption. Therefore the inks behave differently on every surface. Furthermore, the number of cases in three-ink-printing ($N = 1290$) is too large for performing exhaustive measurements.

We propose a simplified model of ink spreading. First, the geometry of the problem is simplified.^{15,16} The hexagon is subdivided into six triangles which share the centre O of the hexagon as a common vertex (see Figure 5). Second, the spreading in the direction of the mediator of the segment $[a, b]$ is supposed to depend only on the state of the neighbours located in a and b , and the state of the surface at the centre O of the hexagon.

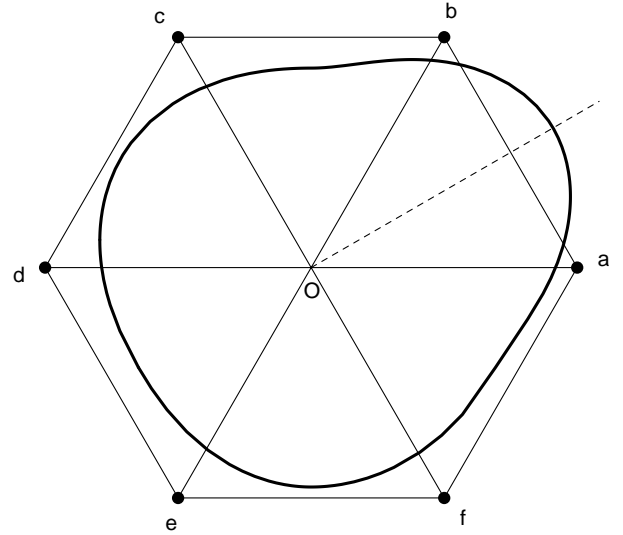


Figure 5. A simplified geometry: the hexagon is subdivided into six triangles which share the centre of the hexagon as a common vertex. The spreading of the ink drop impact in the direction of the mediator of $[a, b]$ depends only on the state of O , a and b .

Table 2: Cycle factorisations and monomials of the group S of symmetries acting on the segment $[a, b]$

Symmetry	Cycle factorization	Monomial
ρ^0	$[a], [b]$	z_1^2
τ_{ab}	$[a, b]$	z_2

This simplified geometry allows to define a group S of symmetries acting on the segment $[a, b]$, because only a and b play equivalent roles in the triangle (a, O, b) . The group S has two elements: ρ^0 the rotation by the null angle, and the reflection τ_{ab} whose axis is the mediator of the segment $[a, b]$. The cycle factorisations and the monomials of the group S are listed in Table 2. The cycle index is:

$$P(z_1, z_2) = \frac{1}{2} \cdot (z_1^2 + z_2) \quad (7)$$

Finally, the total number of non-equivalent configurations is given by combining equation (6) and equation (7):

$$N = (k-1) \cdot P(k, k) = \frac{(k-1) \cdot k \cdot (k+1)}{2} \quad (8)$$

where k is the number of states of a neighbour.

According to relation (8), in two-ink-printing ($k = 3$) we must consider $N = 12$ cases; in three-ink-printing ($k = 4$), we must consider $N = 30$ cases; and in four-ink-printing ($k = 5$), we must consider $N = 60$ cases.

These sets of cases are small enough for performing exhaustive measurements in order to calibrate the ink spreading model. From each case, we can deduce the value of a coefficient r_i which is used by our impact model defined previously. The shape of a simulated impact depends on six r_i coefficients which are related to the configuration of the neighbouring impacts and the state of the surface.

Enumerating the configurations

Pólya's counting theory gives the number of configurations which must be considered in order to calibrate the ink spreading model. The configurations themselves are computed by other means. There are powerful generating algorithms,¹⁴ but for the sake of simplicity, a naive sieve method is used. The computer generates the list of all configurations. Considering the first configuration, all equivalent configurations are removed from the list. The computer applies this procedure to the next configuration of the list until the end of the list is reached. The 12 non-equivalent configurations for two-ink-printing are listed in Figure 6.

Prediction results and discussion

The new ink spreading model was combined with our colour prediction method⁶ in order to predict the spectra of six series of 25 samples. Each series was printed using two inks. All series were produced with a clustered dither algorithm with 33 tone levels. Three series were printed with an HP-DJ560C printer on "Ilford Inkjet Photo Paper",⁷ and three series were printed with an EPSON Stylus Color printer on "EPSON glossy photo quality" paper.

The ink spreading coefficients are given in Figure 6. For each ink-paper combination, the radius r_0 of an isolated circular impact was measured accurately under the microscope. The corresponding coefficients r_i were estimated visually under the microscope, and tuned for five samples by several simulation iterations.

Using our method we computed the spectra of 150 samples. The prediction results are encouraging: the average prediction error between computed spectra and measured spectra is about $\Delta E = 2$ and the maximal error is $\Delta E = 5.5$ in CIE-LAB (see Table 3).

	HP	EPSON		HP	EPSON
	$r=1.$	$r=1.$		$r=1.15$	$r=1.$
	$r=1.1$	$r=1.$		$r=1.2$	$r=1.1$
	$r=1.$	$r=1.$		$r=1.6$	$r=1.2$
	$r=1.$	$r=1.$		$r=1.2$	$r=1.2$
	$r=1.$	$r=1.$		$r=1.6$	$r=1.2$
	$r=1.$	$r=1.$		$r=1.05$	$r=1.05$

Figure 6. List of the 12 non-equivalent configurations in a two-ink-print. The dashed circles indicate the locations of neighbours which are not covered with ink. The white disks correspond to one ink drop, and the black disks correspond to two ink drops.

The vectors indicate the orientation of the spreading. The magnitude of the spreading of HP-inks printed on Ilford paper and the magnitude of the spreading of EPSON-inks printed on EPSON paper are respectively given in the columns entitled HP and EPSON, where $r = r_i/r_0$.

Table 3: Prediction results in CIELAB

Series	ΔE	$\sqrt{\frac{\sum \Delta E^2}{n}}$	Maximal ΔE
Cyan-Magenta on HP printer	2.88	3.21	5.53
Cyan-Yellow on HP printer	2.03	2.38	5.38
Magenta-Yellow on HP printer	1.67	1.80	2.67
Cyan-Magenta on EPSON printer	1.72	1.92	4.26
Cyan-Yellow on EPSON printer	1.98	2.21	4.18
Magenta-Yellow on EPSON printer	1.59	1.77	3.11

The magenta ink of the HP printer is fluorescent. Therefore an advanced spectral prediction model⁴ was used to compute the spectra of the samples produced with this ink. Since fluorescence is out of the scope of this article, we focus the discussion on the Cyan-Yellow samples.

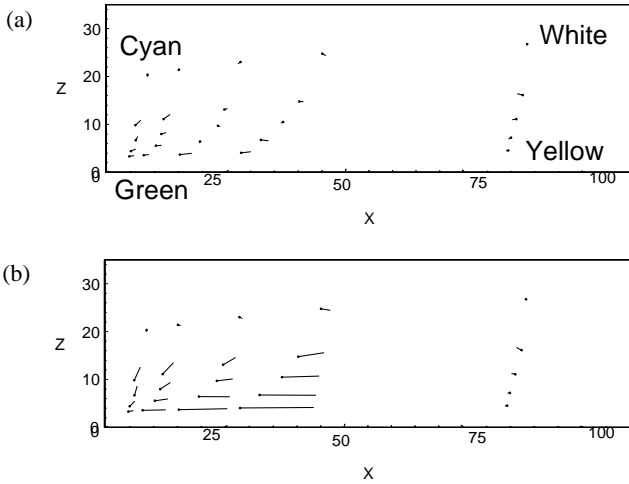


Figure 7. Deviations between computed and measured colours of 25 samples in CIE-XYZ space: (a) taking ink spreading into account, (b) without taking ink spreading into account. The dot indicates the measured colour, and the other end of the segment indicates the computed colour. The 25 samples were printed with cyan and yellow inks on Ilford paper using an HP DJ560C printer.

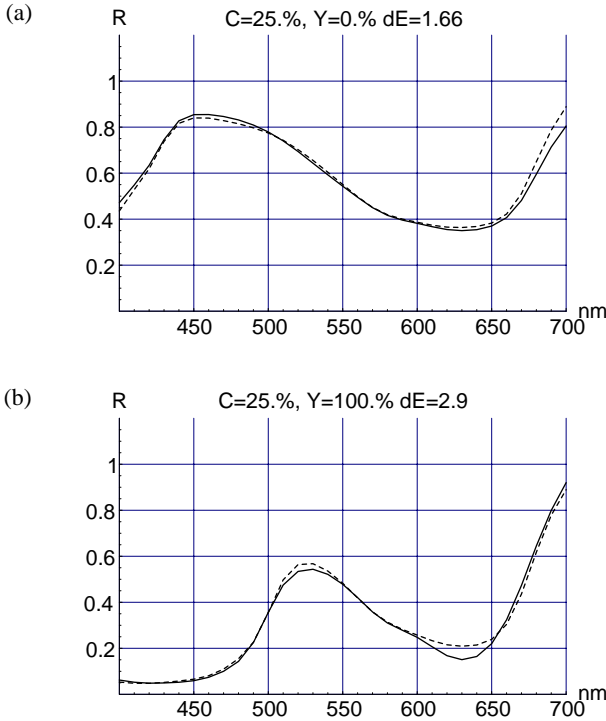


Figure 8. Measured spectra (continuous lines) and predicted spectra (dashed lines) of the halftoned cyan sample shown in Figure 1a (25% ink coverage), and of the green sample shown in Figure 1b (superposition of a cyan layer at 25% ink coverage and a yellow layer at 100% ink coverage).

Figure 7 shows how our ink spreading model improves colour prediction. We consider 25 samples printed with cyan and yellow inks on Ilford paper with an HP DJ560C printer. The measured and computed spectra of the 25 samples are converted into CIE-XYZ values. Figure 7a shows the deviation between measured and computed colours taking ink spreading into account; and Figure 7b shows the deviation between measured and computed colours without taking ink spreading into account. The spectra of samples made with only one ink are well predicted because almost no ink spreading occurs (samples in the white-yellow and white-cyan colour domain). Without taking ink spreading into account, the prediction error is higher than $\Delta E = 10$ in CIELAB for samples made of two inks, since ink spreading is favoured by printing ink drops one over another. Therefore, we have large deviations for samples in the cyan-yellow-green colour domain.

The measured and predicted spectra of the cyan and green samples presented respectively in Figure 1a and Figure 1b are given in Figure 8a and Figure 8b. Remember that sample (b) is made of the same cyan layer as sample (a) and covered with a uniform yellow layer. In spite of the absence of absorption of the yellow ink at 630nm, the measured reflection coefficient of sample (b) is lower than the one of sample (a) at this wavelength (compare Figure 8b and Figure 8a). This difference is explained by ink spreading. The cyan ink covers a larger area with a lower density, and therefore produces a higher light absorption. Note that in the case of sample (b), the prediction error is about $\Delta E = 23$ if ink spreading is not taken into account.

Conclusions

We introduced a new method for investigating ink spreading. The spreading process was modelled by enlarging the drop impact according to the configuration of its neighbours and the state of the surface. The number of cases which must be analysed is reduced to a small set by using Pólya's counting theory. In a three-ink-printing process, only 30 cases must be considered instead of $3 \times 4^6 = 12288$. In a two-ink-process, this figure goes down to 12 cases instead of $2 \times 3^6 = 1458$.

The printing process was simulated by stamping impacts of different shapes on high resolution grids. Each shape is determined by 6 radii. The values of each radius are estimated by a visual observation of the cases given by Pólya's counting theory. This allowed us to compute the relative areas occupied by the various ink combinations in a two-ink-process. We predicted accurately the spectra of 150 samples produced by two different printers. The average prediction error is about $\Delta E = 2$ and the maximal error is $\Delta E = 5.5$ in CIELAB.

Our ink spreading model can also improve advanced Neugebauer-based colour prediction methods since they require an accurate estimation of the area covered by each ink combination. Currently we are extending our investigation to three-ink combinations.

Appendix: Total amount of dye within an ink drop impact

The density profile of an ink drop impact is given by equation (2). The total amount T of dye within an ink drop impact is obtained by integrating equation (2) over the area covered by the impact:

$$T = \int_0^{2\pi} \int_0^{r(\theta)} \left(D_M \cdot \left[1 - \left(\frac{\rho}{r(\theta)} \right)^2 \right] \right) \rho d\rho d\theta \quad (9)$$

During the spreading process, the amount of dye T remains constant. We can establish a relation between the maximal density D_0 at the centre of a drop which did not spread, and the density D_M at the centre of a drop which spread, by calculating T in both cases.

Within an isolated circular impact ($r(\theta) = r_0$) which did not spread ($D_M = D_0$), the total amount of dye is:

$$T = \frac{\pi}{2} \cdot D_0 \cdot r_0^2 \quad (10)$$

Let us now consider an ink drop which spread. In this case, $r(\theta)$ is defined piecewise as shown in equation (1). The integral in equation (9) can be written:

$$T = \sum_{i=1}^6 \int_{\theta_i}^{\theta_{i+1}} \int_0^{r(\theta)} \left(D_M \cdot \left[1 - \left(\frac{\rho}{r(\theta)} \right)^2 \right] \right) \rho d\rho d\theta \quad (11)$$

where $\theta_i = \frac{\pi}{6} + (i-1) \cdot \frac{\pi}{3}$. By integrating in equation (11) with respect to variable ρ , we get:

$$T = D_M \sum_{i=1}^6 \int_{\theta_i}^{\theta_{i+1}} \frac{[r(\theta)]^2}{4} d\theta \quad (12)$$

In the next step, the following change of variable is performed: $t = (3/\pi)(\theta - \pi/6) - i$. The integral (12) can be written:

$$T = \frac{\pi \cdot D_M}{12} \sum_{i=1}^6 \int_0^1 [2(r_i - r_{i+1})t^3 - 3(r_i - r_{i+1})t^2 + r_i]^2 dt \quad (13)$$

By integrating in equation (13) with respect to variable t , we get:

$$T = \frac{\pi \cdot D_M}{12} \sum_{i=1}^6 \left(r_i r_{i+1} + \frac{13}{140} \cdot (r_i - r_{i+1})^2 \right) \quad (14)$$

Finally, by combining equations (10) and (14) we obtain relation (3).

Acknowledgment

We would like to thank Dr. Rita Hofmann from Ilford Imaging for providing useful information on ink-jet paper, and the Swiss National Science Foundation (grant No. 21-54127.98) for supporting the project.

References

1. R. A. Brualdi, *Introductory Combinatorics*, Third Edition, Prentice Hall, London, 1999, pp. 546-586.
2. R. A. Brualdi, *Introductory Combinatorics*, Third Edition, Prentice Hall, London, 1999, p. 575.
3. P. Emmel, *Modèles de Prédiction Couleur Appliqués à l'Impression Jet d'Encre*, PhD thesis No. 1857, Ecole Polytechnique Fédérale de Lausanne (EPFL), Lausanne, Switzerland, 1998, p. 114, <http://diwww.epfl.ch/w3lsp/publications/colour/thesis-emmel.html> (in French).
4. P. Emmel, R.D. Hersch, "Spectral Colour Prediction Model for a Transparent Fluorescent Ink on Paper," *Proceedings of the 6th IS&T/SID Color Imaging Conference*, Scottsdale, Arizona, November 17-20, 1998, pp. 116-122.
5. P. Emmel, R.D. Hersch, "Towards a Color Prediction Model for Printed Patches," *IEEE Computer Graphics and Applications*, Vol. **19**, No. 4, July/August 1999, pp. 54-60.
6. P. Emmel, R.D. Hersch, "A Unified Model for Color Prediction of Halftoned Prints," *Journal of Imaging Science and Technology*, Vol. **44**, No. 4, 2000, pp. 351-359.
7. <http://www.ilford.com/>
8. P. Kubelka, F. Munk, "Ein Beitrag zur Optik der Farbanstriche," *Zeitschrift für technische Physik*, Vol. **12**, 1931, pp. 593-601.
9. S. Lang, *Algebra*, Third Edition, Addison-Wesley, New York, 1995, p. 7.
10. S. Lang, *Algebra*, Third Edition, Addison-Wesley, New York, 1995, p. 30.
11. G. Pólya, "Kombinatorische Anzahlbestimmungen für Gruppen, Graphen und chemische Verbindungen," *Acta Mathematica*, Vol. **68**, 1937, pp. 145-254.
12. G. Pólya, R. C. Read, *Combinatorial Enumeration of Groups, Graphs and Chemical Compounds*, Springer, New York, 1987.
13. R. Rolleston, R. Balasubramanian, "Accuracy of Various Types of Neugebauer Model," *Proceedings of the First IS&T/SID Color Imaging Conference*, Scottsdale, Arizona, November 1993, pp. 32-37.
14. J. Sawada, *Fast Algorithms to Generate Restricted Classes of Strings Under Rotation*, PhD thesis, University of Victoria, Canada, 2000.
15. S. Wang, "Algorithm-Independent Color Calibration for Digital Halftoning," *Proceedings of the Fourth IS&T/SID Color Imaging Conference*, Scottsdale, Arizona, November 19-22, 1996, pp. 75-77.
16. S. Wang et al., United States Patent Number 5,748,330, May 5, 1998.